

Integration of recent drill results with multichannel seismic data: New inferences on the subsurface configuration and sedimentary history of the northwestern Bay of Bengal

Maria Desa^{1,2,*}, Jensen Jacob^{1,2,*}, Walsh Fernandes¹, Saif Ali Khan^{1,2}

¹CSIR-National Institute of Oceanography, Dona Paula, Goa-403004, India

²Academy of Scientific and Innovative Research (AcSIR), Ghaziabad-201002, India

*corresponding authors: mdesa@nio.org; jacob@nio.org

Abstract

The study pertains to the use of two industry wells and one IODP drill site in conjunction with high quality multichannel seismic data in the northwestern Bay of Bengal. The industry wells provide subsurface information from Early Cretaceous period while the IODP drill site U1444 gives information about deposition younger to Miocene. Their locations over the seismic profiles facilitated the assignment of ages to the prominent seismic horizons thereby yielding a revised seismic stratigraphy of the northwestern Bay of Bengal.

The ages of the oldest seismic horizons are in agreement with the recently published ages of the underlying oceanic crust. The sediments up to Late Cretaceous time are thick west of 85°E Ridge, while to its east, they are thin. The sediments up to Paleocene time thin towards offshore, implying that they are land derived (from East Coast of India). Fan sedimentation commenced in the Eocene time and was excessive since Miocene. The transparent sequence between the Late Pleistocene and Pliocene unconformities is thin over the 85°E Ridge. The western extents of the Quaternary subfans above the Late Pleistocene unconformity are demarcated in the study area.

Further, the study suggests that the emplacement of the 85°E Ridge took place in the Middle Cretaceous period. Faulting/folding at the continental rise occurred around Miocene time and maybe linked to intraplate deformation that occurred in the Central Indian Ocean Basin. Thus, the inferences drawn from this study help to provide a reliable sedimentary history of the northwestern Bay of Bengal forming an updated base for future investigations.

1. Introduction

The Bay of Bengal (Figure 1) lying off the East Coast of India, is floored by the world's largest submarine fan, the Bengal Fan (Curray et al., 1982). A network of turbidity channels distributes the enormous sediment input from the Ganga-Brahmaputra river system up to south of the equator (Curray et al., 2003). Further, the sediment distribution pattern has been affected by the N-S trending 85°E and Ninetyeast Ridges (Curray, 1994).

The Bay of Bengal has been studied considerably for its various exceptional processes and tectonics. However, some vital parameters like age and nature of the crust/overlying sediments, ridge emplacement mechanisms, etc. are still debated. Moreover, multiple theories are proposed for a single event, process or structure. One such matter is the seismic stratigraphy of the Bay of Bengal. Either the seismic stratigraphy has been done in isolation in a particular area, or the ages assigned to the horizons differ considerably due to lack of correlation with a drill site.

Recent results have assigned reliable crustal ages for the oceanic crust underlying the Bay of Bengal (Talwani et al., 2016; Desa and Ramana, 2016). Further, drill data has been freshly acquired by IODP and industry for solving crucial scientific problems and hydrocarbon prospecting, respectively. An integrated study incorporating the updated crustal ages and revised seismic stratigraphy based on recent drill results has not been attempted before.

Detailed integration of available multichannel seismic data and recent drill results, helped to identify the major seismic horizons and validate their ages. Prominent (Paleocene, Pliocene and Late Pleistocene) unconformities are identified and Quaternary subfans are inferred in the northwestern Bay of Bengal. Thereby the seismic stratigraphy is updated and the sedimentary history is traced. Further, the role of 85°E Ridge (85ER) in the depositional history in the northwestern Bay of Bengal is discussed.

2. Geological Background

The oceanic crust of the Bay of Bengal (Figure 1) was formed due to the breakup of Eastern Gondwanaland, and subsequent seafloor spreading between Greater India and Antarctica-Australia since the Early Cretaceous (Powell et al., 1988; Ramana et al., 1994; Talwani et al. 2016). This spreading occurred in two episodes: the first occurred passively in the NW-SE direction and formed the oceanic crust since 132 Ma (Talwani et al., 2016). The second breakup episode occurred in the Middle Cretaceous after the Kerguelen plume arrived beneath eastern India (Kent, 1991) causing the eastern portion of the spreading ridge to jump to the Rajmahal-Sylhet traps along a longitudinal crack (Talwani et al. 2016). Spreading was initiated in the eastern basin of the Bay of Bengal (Desa

and Ramana, 2016), and the spreading direction changed to N-S by 100 Ma (Matthews et al., 2012). By the Late Cretaceous, full-fledged spreading (Royer and Sandwell, 1989) occurred with major transform activity along the 86E°/Kerguelen Fracture Zone.

The buried 85ER (Figure 1) has been inferred based on seismic records and its typical gravity signature (Curry et al., 1982; Liu et al., 1982). It is described in detail later in the text. The Ninetyeast Ridge is one of the longest linear topographic features in the world, along the 90°E meridian (Heezen and Tharp, 1964). The ridge is visible south of 10°N (Figure 2), and is inferred to be buried under the fan sediments in the north (Curry et al., 1982). It is considered as the trace of the Kerguelen plume as the Indian plate moved northwards (Duncan, 1991).

Conventional sedimentation occurred in the Bay of Bengal till Paleocene time over the oceanic crust generated at high southern latitudes (Davies and Kidd, 1977). The rapid northward movement of Greater India in the Paleocene ended due to its 'soft' collision with Eurasia in middle Eocene (Patriat and Achache, 1984; Lee and Lawyer, 1995) causing a major change in sedimentation pattern in the Bay of Bengal (Moore et al., 1974; Cochran, 1990). Hard collision of Greater India with Eurasia (Replumaz and Tapponnier, 2003) resulted in the uplift of the Himalayas causing huge amount of sediments to enter the Bay of Bengal as fan deposits by Oligocene time (Moore et al., 1974). Monsoon activation in the Miocene resulted in intense erosion of the Himalayas and deposition of clastics at high rates of 5-10 cm/kyr (France-Lanord et al., 1993; Clift et al., 2008). Continued erosion of the Himalayas and Indo-Burma Ranges (Alam et al., 2003) together with sea level changes since Pliocene (Haq et al., 1987) caused increased but irregular deposition of coarse turbidites and hemipelagics (Weber and Reilly, 2018).

2.1 Seismic stratigraphy

The Bengal Fan is the world's largest submarine fan formed by huge influx of clastic sediments moderated by sea-level fluctuations, climate change, and source area tectonic activity (Curry et al., 2003). Turbidite sedimentation is the dominant process by which the clastic material is transported from land into the fan. Conventionally this sedimentation occurs at low sea levels (Shanmugan and Muiola, 1982), while at high sea levels, hemipelagic sedimentation is observed (Bouma, 2001). These changes in sedimentation are manifested as strong reflectors in seismic records.

Seismic stratigraphy of the Bay of Bengal was first reported by Curry and Moore, (1971), with the identification of W, Y and O units separated by unconformities. The age of the older unconformity was concluded at DSDP217 as late Paleocene to middle Eocene after which the fan was initiated (Curry and Moore, 1974). Based on seismic reflection, refraction and wide-angle reflection studies,

Curray et al. (1982) identified major reflectors as Q (Quaternary-Pliocene contact), M (regional Upper Miocene unconformity) and P (Paleocene-Eocene unconformity). The P unconformity demarcates the sediments deposited before and after the collision of Greater India with Eurasia in the middle Eocene. This unconformity represents a period of non-deposition or greatly reduced rate of deposition (hiatus), and forms the base of the Bengal Fan (Curray et al., 1982). Continued collision of Greater India with Eurasia resulted in intraplate deformation in the Central Indian Ocean Basin, whose onset is seen as the M reflector on seismic records (Curray and Munasinghe, 1989).

Eight horizons were identified on profile SK31 along 13°N (Gopala Rao et al., 1994) based on correlation with the Q, M and P unconformities of Curray et al. (1982) (Figure S1). Five latitudinal multichannel seismic profiles were used to infer four unconformities (lower Eocene P, Oligocene, Miocene A, upper Pleistocene B) in the Bay of Bengal (Gopala Rao et al., 1997) (Figure S1). Transparent sequences were interpreted as fine grained sediments. Further, the presence of turbidites was inferred since Oligocene. Bastia et al. (2010) investigated the seismic profiles in the Mahanadi offshore basin, and identified O-T and K-T reflectors around the 85ER. Multichannel seismic profiles SK107-07 and SK107-06 (Figure S1) were analysed for seismic stratigraphy, and the four major reflectors identified on these profiles (Michael and Krishna, 2011) are similar to those reported by Gopala Rao et al. (1997).

Major seismic horizons/unconformities were identified in the Mahanadi offshore, based on the interpretation of Curray et al. (1982) by Desa et al. (2013) (Figure S1). Thicker older sediments were inferred west of 85ER as compared to east of the ridge. Krishna et al. (2016) inferred two phases of deposition: the first phase occurred till 23 Ma at relatively low sedimentation rates, and the second phase thereafter having high rates with input sourced from the Ganga-Brahmaputra river system.

Two regional unconformities were inferred along 8°N and were interpreted to be of Pliocene (4.8 Ma) and Late Pleistocene (0.64 Ma) age (Von der Borch et al., 1974; Schwenk and Spiess, 2009). The sedimentation rates were highest in the Pleistocene, lowest in the Pliocene, and moderate in the late Miocene (Schwenk and Spiess, 2009). Further, two angular unconformities U_c and U_d were identified along 14°N, wherein the sandwiched unit over the 85ER is fairly thin. These unconformities were validated by the IODP site U1444 as Pliocene (3.6 Ma) and Late Pleistocene (~0.4 Ma) (Clemens et al., 2016). The IODP site U1444 also revealed that the absence of fan sediments between U_c and U_d is a local phenomenon due to the 85ER. Four angular unconformities U_e , U_f , U_g and U_h were inferred along 17°N (Schwenk and Spiess, 2009). U_e and U_f dip westward and are characterized with continuous onlapping, while U_g and U_h are nearly horizontal towards east.

2.1.1 Quaternary Subfans

Fan sedimentation continued into the Quaternary and was influenced by sea-level fluctuations, climate change, and source area tectonic activity (Curry et al., 2003). The turbidity currents cause deposition of thick channel-levee deposits while major shifting of the submarine canyon/channel results in migration of the depocenter leading to the formation of subfans over time.

The concept of subfans in the Bay of Bengal was first introduced by Curry et al., (2003). Four subfans A (1.9 to 0.96 Ma), B (0.96 to 0.465 Ma), C (0.465 to 0.125 Ma), and D (0.125 Ma to date) were inferred within the Pleistocene upper fan sediments, using seismic stratigraphy and correlation to DSDP site 218. Further, they demarcated the extent of these subfans north of 16°N. The oldest subfan A is located around the central region; while during subfan B, four fan lobes were proposed (Curry et al., 2003). Subfan C deposition took place only in the east, while the recent subfan D is located south of 18°N (Figure S2).

Bergmann et al. (2019) extended the subfans southward up to 8°N and refined their timings as follows: B (1.24 to 0.68 Ma) during Middle Pleistocene; C (0.68 to 0.25 Ma) seen in the east; and D (0.25 Ma to date) during Late Pleistocene (Figure S2). They inferred that along 14°N, subfan D onlaps subfan C towards east. Further, they suspected the presence of subfan B below U_c , the base of subfan C. Along 17°N, they proposed that U_e and U_f enclose subfan C, which is onlapped by subfan D towards east. Here they suspected that subfan B lies between U_f and U_g . Their oldest subfan B extends east of the 85ER in the north, and west of the ridge in the south. Their subfan C lies entirely east of the 85ER, while their recent subfan D occupies the central region in the north and extends west in the south (Figure S2).

2.2 The 85ER

The buried 85ER is seen on seismic records aligned nearly N-S along 85°E longitude (Figure 1). Curry and Munasinghe (1991) linked its origin to the Crozet hotspot and deduced its age between 117 and 84 Ma. Further, they proposed that the ridge turns westward south of 5°N, and then joins the Afanasy Nikitin seamount chain. Contrastingly, Kent et al. (1992) proposed that it is a northward continuation of the 86°E fracture zone. Ramana et al. (1997) suspected that the 85ER may have formed due to volcanic emplacement during the Middle Cretaceous major plate reorganization. Krishna (2003) proposed that the 85ER may have formed by an unknown hotspot between 85 and 60 Ma. The presence of onlapping sediments of Cretaceous and Paleocene age on either side of the 85ER, indicates its existence prior to their deposition (Bastia et al., 2010). The ridge is proposed to be comprised of at least two segments based on its evolutionary tectonics. The northern portion of

the 85ER is considered to have formed due to volcanism in the Middle Cretaceous period over the longitudinal crack/transform fault along which the spreading ridge jumped north around M0 time (Desa et al. 2013; Talwani et al., 2016). The ridge, south of 12°N, is proposed to be the northward continuation of the 86°E fracture zone (Desa and Ramana, 2016). Based on OBS results, Altenbernd et al. (2020) proposed that the 85ER does not turn westward and is the northward continuation of the 86°E fracture zone.

Nayak et al. (2011) argued that the 85ER was emplaced over the pre-existing oceanic crust, and the pre-ridge sediments must have been buried under the volcanic basement generated by plume activity. Choudhuri et al. (2014) suggested that the volcanism forming the ridge began at 107 Ma in the Mahanadi Basin with basaltic eruptions building giant subaerial and marine volcanoes depressing the lithosphere. The ridge is attributed to magmatism along a fracture zone with age of 105 Ma at the drill site AA (Siawal et al., 2015).

The ridge was initially subaerial and acted as local provenance, and its presence had significant influence on sediment dispersal pattern until Oligocene time (Nayak et al., 2011). The Paleocene and Eocene sequences wedge out against the ridge with chaotic reflections indicating high energy shallow conditions (Dangwal et al., 2008). The ridge got submerged with the global sea level rise during Eocene and its crest remained in shallow (a few 100 meters) waters up to Oligocene as indicated by the 50 m of limestone of Oligocene age at the drill site AA (Siawal et al, 2015; Gorain and Sachdeva, 2017). Complete burial of 85ER took place in Oligocene time as inferred by parallel/sub-parallel seismic reflections sealing the chaotic facies of earlier sequences (Dangwal et al., 2008).

2.3 Intraplate deformation

Intraplate deformation has been reported in the Central Indian Ocean Basin (Wiens et al. 1985; Gordon et al., 1998) based on high seismicity, unusual heat flow, gravity/geoid anomalies and seismic records (Weissel et al., 1980; Geller et al., 1983). The compressional stress due to the collision of India with Eurasia, resulted in east-west striking folds and thrust faults, west of Ninetyeast Ridge (Wiens et al., 1985). East of Ninetyeast Ridge, this deformation is seen mostly as left lateral strike slip motion (Depluse et al., 1998). Deformation began around Miocene time (Weissel et al., 1980) and caused a major unconformity (M) separating the pre and syn-deformational sediments, throughout the Bay of Bengal (Curry and Munasinghe, 1989). Recent episodes are inferred in Pliocene and Pleistocene times too (Krishna et al., 2001).

3. Methodology

The present study incorporates high quality multichannel seismic profiles off the East Coast of India, acquired by ION/GX Technology. The data was acquired using air guns with source volume of 7,510 cubic inches, with a shot point interval of 50 m and group interval of 25 m. The streamer length was 10 km and the sampling rate was 2 msec giving 100-fold coverage. The pre-stack time migrated sections are used in the present study.

Two wells K-1 (Krishna et al., 2016) and AA (Siawal et al, 2015; Gorain and Sachdeva, 2017) drilled by ONGC in the Bay of Bengal, lie on the seismic dip profile GXT1290 at #6900 and #2800 respectively (Figure 2). K-1 lies off the East Coast of India (16.7965°N, 83.6326°E), while AA is located on the 85ER (15.4708°N, 84.9659°E). The drill information in the form of lithology and ages, at drill sites K-1 and AA are described in Tables 1 and 2 respectively.

The subsurface layers provided by the drill data were correlated with the prominent seismic sequences on the seismic record GXT1290 by generating a synthetic seismogram (Figure S3, supplementary information). Further, the age information was used to date the prominent horizons on the seismic record GXT1290 (Figure 3; Tables 1 and 2). Thus, the horizons corresponding to the Top of Miocene (H7), Top of Oligocene (H6), Top of Eocene (H5), Paleocene Unconformity (H4), Top of Late Cretaceous (H3), Top of Middle Cretaceous (H2) and Top of Early Cretaceous (H1) were identified on the above seismic profile. Further, the subsurface layers at the drill sites were decompacted to calculate the sedimentation rates at different times (supplementary information). We mention here that our correlation of well K-1 with GXT1290 exhibits consistent interval velocities, includes the Paleocene unconformity and differs slightly from that of Krishna et al. (2016).

Additionally, the drill results at IODP site U1444, Leg 353 (14°N, 84.829°E) (Clemens et al., 2016) were used to identify the horizons younger than Miocene (Table 3). Site U1444 lies on the seismic profile GeoB97-041 along 14°N on which two major unconformities U_c and U_d were marked (Schwenk and Spiess, 2009). These unconformities were validated by the site U1444 as Late Pleistocene (~0.4 Ma) and Middle Pliocene (3.6 Ma) unconformities (Clemens et al., 2016).

The seismic profile SK107-07 extending between 83.35°E and 91.92°E (Michael and Krishna, 2011) along 14°N, overlaps the profile GeoB97-041 (Figure 2). The unconformities U_c and U_d were thus marked on the profile SK107-07 (Figure 4) which in turn ties with the profiles GXT1100 and GXT1200 facilitating the transfer of younger seismic horizon identification (Pliocene and Late Pleistocene Unconformities) to these profiles.

From GXT1290, the validated deeper horizons were transferred to the along strike profile GXT4000 (tie point: #5400/16000) (Figure 5). Likewise, the younger horizons were transferred from profiles GXT1100 (tie point: #5700/10780) and GXT1200 (tie point: #5100/12300) to profile GXT4000. In this manner, the refined seismic horizon identifications were transferred to all the GXT and other seismic profiles in the Bay of Bengal. Thus, a reliable network of age identifications of the seismic horizons was achieved along all the seismic profiles in the northwestern Bay of Bengal. Further, correlation of the northernmost profile GXT1800 with the profile GeoB97-059/069 (Schwenk and Spiess, 2009) and seismic records of Curray et al. (2003) (Figure 2) was done to validate the Quaternary stratigraphy and (and infer the presence of subfans in the study area Curray et al., 2003; Bergmann et al., 2019).

4. Results

The subsurface information obtained from the three drill sites and its correlation with the seismic data helped to identify the prominent seismic horizons, assign ages to them, and compute the sedimentation rates (Tables 1 to 3). Interval velocities range from 1.9 to 2.9 km/sec at the K-1 drill site (Table 1). Sedimentation rates were lower in Oligocene and Eocene times (1.64-2.17 cm/kyr), and increased after Miocene time (15.00 cm/kyr). The interval velocities increase from 2.1 to 3.4 km/sec with depth (Recent to Oligocene) at the AA site (Table 2). Here too, the sedimentation rates increase from Miocene to Recent. At site U1444, the velocities are around 1.6 - 1.7 km/sec (Table 3). Further, this site indicates that the sedimentation rate is least between the Late Pleistocene and Pliocene unconformities, and increases significantly in recent times.

The profile GXT1290 clearly depicts the nine horizons (H1 to H9); the 85ER with a relief of 2.5 sec TWT, and faulting/folding at the continental rise and on either flank of the 85ER (Figure 3). We have tentatively identified older horizons till H6 in the upper continental slope region, which thin at the lower slope. We find that H7 onlaps onto H6, while horizons H4 and H5 onlap onto H3. The deepest horizon H1 (Early Cretaceous top) marks the upper boundary of the transparent sequence lying over the basement. H2 marks the upper limit of the sequence overlying H1 and having relatively higher amplitude. Both these sequences maintain constant thickness (0.5 sec TWT each) west of the 85ER and appear to be absent east of the ridge. The shallowing of horizons H1 and H2 at the western flank of 85ER suggests that the ridge was uplifted after their deposition. The sequence below H3 (Late Cretaceous top) is rather chaotic and wedges at the 85ER, while the unit below H4 (Paleocene Unconformity) truncates against the ridge (Figure 3). The termination of the horizons H3 and H4 against the western flank of the ridge indicates they were deposited after the ridge was

uplifted. East of 85ER, sediments older than H3 are thin (<1 sec TWT in comparison to ~2 sec TWT west of ridge) and appear transparent. The ridge is buried by H6 (Oligocene) time.

The unit below H4 thins eastward, while the unit above it thins westward resulting in a nearly horizontal H5 (Eocene top) reflector (Figure 3). Further, the Eocene sediments onlap onto horizon H4 confirming that H4 is a prominent unconformity. The disposition of these horizons H4 and H5 suggests that an alternate strong sediment source dissipated the existing sedimentary source (adjoining Indian peninsular). The parallel trend of the reflectors from H5 to recent time suggests constant distribution of sediments by the alternate source (fan deposits) from the foot of slope to offshore.

Further, the sequences between horizons H6 (Oligocene top) and H8 (Pliocene unconformity) are manifested as alternate bands of continuous to discontinuous; parallel to sub-parallel, strong and weak reflectors. These reflectors extend along the entire profile and are characterised by several buried channels. The shallower sequences (above H8) are characterised by several transparent zones alternating with highly chaotic zones. Further, the horizons H8 (Pliocene) and H9 (Late Pleistocene) can be considered as major unconformities with younger sequences onlapping onto them.

Neotectonic activity (deformation) is seen at the continental rise along this profile (Figure 3). A large single fault with a throw of about 1 sec TWT occurred around H7 (Miocene) time disturbing the entire sediment column and the underlying crust. This faulting activity continued at least till H8 (Pliocene) time. Minor faulting (0.2 sec TWT) is seen at either flank of the 85ER with similar amount of folding over the ridge. This faulting has dislocated horizons up to Pliocene time. Further, folding of horizons H5 to H7 is observed east of the 85ER (at the eastern flank).

The along strike profile GXT4000 depicts a broad double humped structure encompassing the 85ER (Figure 5). The basement is deeper than 8 sec TWT, with more than 5 sec TWT thick sediments on either side of the ridge. Thick older than H3 sediments are seen immediate southwest of the ridge while they are thin in the northeast. Shallowing of H1 and H2 is seen at the southwestern flank of the 85ER. The truncation of horizon H3 (Late Cretaceous) suggests the ridge existed before the deposition of the underlying unit. Here too, the ridge is buried around H6 (Oligocene) time.

Further, the section indicates thick Eocene (below H5) sediments in the northeast indicating that alternate source sedimentation began by this time (Figure 5). A ~0.5 sec TWT broad uplift of all the horizons along with the 85ER is seen to have occurred at H7 (Miocene top) time. Minor faulting/uplift of the ridge continued as recent as H8 (Pliocene) time. Thick sediments younger to H8 are seen between shots 9000 to 15000 suggesting a recent strong localized source of sediments

(Figure 5). Detailed investigations of the other seismic profiles depicted all the above features and similar subsurface configuration.

Our seismic network facilitated the identification of the unconformities proposed by Schwenk and Spiess (2009) along 17°N (GeoB97-059/069). Correlation of our northernmost seismic profile GXT1800 with the above seismic track indicates that U_g is same as H9, and U_h is same as H8 (Figure 6). Thus, U_g and U_h are the Late Pleistocene (U_c) and Pliocene (U_d) unconformities respectively. The unconformity U_f identified by Schwenk and Spiess (2009) is also seen along our profile GXT1800 as a prominent reflector which we have named as H10.

Our profile GXT1800 crosses the seismic profiles used by Curray et al. (2003) to infer the subfans A to D. We marked these subfans A, B and D on our profile GXT1800 (Figure 6, labelled in red). Further, the subfans B and C proposed by Bergmann et al. (2019) on profile GeoB97-059/069 could be identified on GXT1800. We are now able to make a first-hand comparison of the subfans proposed by Curray et al. (2003) and Bergmann et al. (2019), and we see that there are discrepancies in their inferences.

Subfan A marked by Curray et al. (2003) but not marked by Bergmann et al. (2019), can be confidently extended southward and eastward (Figure 6), and lies between unconformities U_g /H9 and U_h /H8. So, this subfan deposition occurred between the timings of the Pliocene and Late Pleistocene Unconformities. This subfan depicts rather transparent facies in the north, and chaotic facies with thinning towards south and east.

Subfan B is identified by both Curray et al. (2003) and Bergmann et al. (2019), and lies between reflectors H9/ U_g and H10/ U_f (Figure 6). It is highly uneven in thickness and occasionally shows sub-parallel reflections. Wherever the thickness is more, reflections are chaotic.

Subfan C of Bergmann et al. (2019) can be continued northward (Figure 6) as the lower portion of the subfan D of Curray et al. (2003). By terming this lower portion as subfan C, we resolve the discrepancy between the identifications of Curray et al. (2003) and Bergmann et al. (2019). This subfan C lies on H10/ U_f , and is occasionally transparent in the north, while it gets chaotic towards south. It thins further east (Figure 6).

Subfan D is the uppermost layer seen throughout our profile GXT1800. It is the most recent layer being deposited till date. At places, it depicts truncation/incision by the channels, while at other places it has parallel reflectors (Figure 6).

The subfan interpretation was extended onto our entire seismic network which facilitated inferring the presence of the subfans in the study area. Figure 7 is a seismic record belonging to the profile

GXT1240, just north of profile GeoB97-041 (Figure 2). It depicts the subfan B overlapping onto H9 and wedging eastward. Subfan D is seen nearly flat with two small surface channels, one of them (at #1900) was large and is recently buried. Further, the sequence between the horizons H9 and H8, is transparent. Horizons older to H8 are seen folded and multiple faulted at the western flank of the 85ER. These faults have occurred since H7 (Miocene) time, with an episode in Pliocene (black arrow). Another episode occurred in late Pliocene (green arrow), forming a scarp which caused the subsequent sediments to wedge against it (Figure 7). Yet another faulting episode is seen between the horizons H9 and H8.

The present study indicates that the subfan A is restricted in the north (Figure 8). The subfan B is identified on all the profiles and wedges on H9 above the 85ER as seen in Figure 7. Subfan C is seen as a thin layer towards east, and is absent west of 85ER (Figure 8). The recent subfan D is seen on all the profiles and it occurs more east when compared to subfan B. The sediment thickness above H9 (Late Pleistocene) is maximum (up to 0.8 sec TWT) in the north (Figure 8). Off Krishna-Godavari coast, it reaches to 0.4 sec TWT. Along the 85ER, these sediments are relatively less (up to 0.1 sec TWT).

5. Discussion

Our seismic horizon interpretation was compared to previously published seismic identifications (Figure S1) (Gopala Rao et al., 1994; 1997; Bastia et al., 2010; Michael and Krishna, 2011; Desa et al., 2013; Krishna et al., 2016). Along the profile SK31 (Gopala Rao et al., 1994), their identifications differ from our interpretation to some extent. Comparison of our seismic horizon interpretation with that along the E-W profiles in the Bay of Bengal (Gopala Rao et al., 1997) revealed that their Upper Miocene (A) is too shallow, and Pliocene Unconformity was not identified at all. Along profiles SK107-07 and Sk107-06 running along 14°N and 15.5°N respectively (Michael and Krishna, 2011), their Upper Pleistocene is quite deep, while their Upper Miocene is rather shallow. Comparing our results with those of Bastia et al. (2010), we note that their O-T is nearly similar to our H6 (Oligocene), but their K-T is incorrect on some profiles. On comparison of our identifications with that of Desa et al. (2013), it is noted that their M matches our Pliocene H8, and their P is our H6 Oligocene top. Our horizon identifications and sedimentation rates were compared with those of Krishna et al. (2016) and minor differences were noted.

Thus, the published identifications differ considerably amongst themselves as well as with those made in the present study. Further, the vertical resolution of the published sections was inadequate, while the seismic records used in this study are of high quality. Considering the limitations of the

published identifications, it is clear that the present identifications based on drill results are concrete and may be considered as valid constraints for future work in the northwestern Bay of Bengal.

Along the strike line GXT4000, the oldest seismic horizons are H1 and H3, southwest and northeast of the 85ER respectively (Figure 5). Moreover, thick older (below H3) sediments are seen southwest of the 85ER, while this pack is thin to its northeast. Considering this profile is equidistant from the coast throughout its length (Figure 2), it implies that the northeastern portion of the basement could be younger in age. This is in agreement with the recently published ages of the underlying oceanic crust in the Bay of Bengal (Talwani et al., 2016; Desa and Ramana 2016), that Early Cretaceous crust occurs west of the 85ER, while younger Middle Cretaceous crust occurs to its east (Figure 9a). The shallowing of H1 (Early Cretaceous) and H2 (Middle Cretaceous) at the western flank of the 85ER, together with the truncation of horizon H3 (Late Cretaceous) indicates the ridge was uplifted after the deposition of H2 and before the deposition of H3. This implies that the ridge was evolved in the Middle Cretaceous period.

Deformation in the form of folding and faulting, seen along some seismic profiles off the East Coast of India (Figure 3) has occurred since Miocene time. These signatures lie on the NW-SE trending band of high-magnitude maximum horizontal stress inferred by Muller et al. (2015). The (<20 Ma) age inferred for the growing tectonic stress field is in agreement with the Miocene age for the deformation inferred in this study. Thus, these signatures can be correlated to the intraplate deformation occurring in the Central Indian Ocean Basin (Weissel et al., 1980; Gordon et al., Gordon et al., 1998). The observed doming/faulting/folding of the younger horizons on the 85ER may be attributed to this deformation.

The present study asserts that alternate source sedimentation began in the Eocene time in the study area. This sedimentation belongs to the Bengal Fan (Curry and Moore, 1971). Sedimentation was excessive during Miocene time with high rates of deposition (Tables 1 to 3). Further, higher rates are seen above Late Pleistocene unconformity after a fall during Pliocene time. These rates are similar to those inferred by Schwenk and Spiess (2009) and at U1444 (Clemens et al., 2016). Thick younger sediments seen above horizon H8 and between shots 9000 to 15000 (Figure 5) are due to higher sedimentation rates in the Krishna-Godavari Basin (Rao, 2001).

5.1 Characterisation of the unconformities

The unconformities U_c and U_d proposed by Schwenk and Spiess (2009) along 14°N were confirmed as Late Pleistocene and Pliocene unconformities respectively (Clemens et al, 2016). But the unconformities U_e , U_f , U_g and U_h along 17°N were not assigned ages due to lack of drill site and/or

seismic records. Our seismic network facilitated the identification of U_g as Late Pleistocene and U_h as Pliocene unconformities (Figure 6). Further, U_f is the base of subfan C and U_e may be the base of subfan D.

The IODP site U1444 revealed that the thin transparent sequence between U_c and U_d seen on seismic records (Schwenk and Spiess, 2009) is hemipelagic sedimentation (Clemens et al., 2016). This sedimentation was attributed to the tectonics related to the 85ER. Further, this transparent sequence associated with hemipelagic deposition indicates fan inactivity (Weber and Reilly, 2018). Similar setting is observed along the profile GXT1240 wherein the 85ER and transparent sequence is seen (Figure 7). The present study indicates that this scenario occurs all along the ridge. Further, we observed that this transparent sequence gets rarely chaotic and thicker in the west, away from the ridge. Thus, we suspect that the thickness and character of this transparent sequence may be controlled by the tectonics of the ridge.

IODP Leg 354 at 8°N revealed that the Late Pleistocene unconformity is associated with a lithological boundary between Middle Pleistocene hemipelagic layer and overlying turbidites (France-Lanord et al., 2016). Further, Bergmann et al. (2019) proposed that the Pliocene and Miocene unconformities also represent a shift from background hemipelagic to fan sedimentation. The present study indicates that the horizons H8 and H9 (proposed by Schwenk and Spiess, (2009) as Pliocene and Late Pleistocene unconformities) are characterised by typical features such as onlapping elsewhere, and hence are unconformities in addition to being lithological boundaries (Figure 7).

5.2 Western extent of the Quaternary Subfans

The present study helped to bring a consensus between the inferences by Curray et al. (2003) and Bergmann et al. (2019) on Quaternary subfans A to D. The discrepancy in the identification of subfan C by Curray et al. (2003) and Bergmann et al. (2019) was sorted by terming the lower portion of subfan D of Curray et al. (2003) as subfan C (Figure 6).

Our data suggest the presence of subfan A in the north (Figure 8), as inferred by Curray et al. (2003). The western extent of the subfan B identified by Bergmann et al (2019) has been demarcated using our seismic data. Based on the wedging of subfan B (Figure 7) and its presence on the surrounding profiles, we suggest that this subfan is absent in a limited region on the 85ER (Figure 8). Our identifications of subfan C seen east of 85ER, substantiate those of Bergmann et al. (2019). The western extent of subfan D inferred in this study matches with that inferred by Curray et al. (2003) and Bergmann et al. (2019). The back-and-forth movement of the subfans in the study area is

probably due to the various controlling factors such as sea level fluctuations, climate change, source area tectonics and the presence of the 85ER (Curry et al., 2003; Bergmann et al., 2019).

5.3 The Role of 85ER

The two-episode breakup between Greater India and Antarctica (Talwani et al., 2016) resulted in the formation of Early Cretaceous oceanic crust west of the 85ER, and Middle Cretaceous crust east of the ridge (Desa and Ramana, 2016) as depicted in Figure 9a. Further, it was proposed that the 85ER was emplaced in the Middle Cretaceous over the longitudinal crack/transform fault along which the spreading ridge had jumped north due to plume-ridge interaction (Desa et al., 2013; Talwani et al., 2016).

Our seismic records portray varying shape, relief, morphology, width and character of the 85ER along its length (Figures 3 and 5). The ridge emplacement is attributed to Middle Cretaceous hotspot magmatism ranging from ~107 Ma in the Mahanadi basin (Choudhuri et al., 2014) to 105 Ma at the site AA (Siawal et al., 2015). These ages are in agreement with the Albian and younger ages proposed for the post ridge sediments truncating at the ridge (Nayak et al., 2011). The shallowing of H1 and H2 reflectors, and the truncation of H3 reflector (Figures 3 and 5) at the western flank of the ridge assert that the ridge has indeed formed within the Middle Cretaceous time over pre-existing Early Cretaceous crust. This refutes the claim by Krishna (2003) that the ridge formed from north to south in the Bay of Bengal, between 85 and 60 Ma. The exact source of the ridge volcanism is debatable and beyond the scope of this paper.

The absence of older sediments on the ridge suggests that the ridge formed as a subaerial structure, as indicated by the lava deltas (Choudhuri et al., 2017). Further the presence of more than 50 m limestone of Oligocene age on the ridge indicated that the ridge crest remained in shallow water conditions (Gorain and Sachdeva, 2017). The ridge-basement configuration at 100 Ma (Figure 9b) and the seismic records from this study (Figures 3 and 5) indicate that the 85ER indeed formed as a subaerial structure, remained in subaerial/shallow water conditions till Oligocene, and got buried by Miocene time.

The doming/faulting/folding of the younger horizons at the ridge flanks suggest differential compaction /subsidence or neotectonic activity around the ridge till Pliocene time. The disposition of the subfans is also controlled by the presence of the 85ER and its neotectonic activity (Bergmann et al., 2019). Further, the nature and thickness of the transparent layer between the Late Pleistocene and Pliocene unconformities is influenced by the ridge. Thus one can infer that the ridge has played a significant role in the Bengal Fan sedimentation (Figures 7 and 8).

5.4 Sedimentary history

The northward flight of Greater India from the high southern latitudes to the northern hemisphere since Late Cretaceous involved traversing diverse climate zones (Ali and Aitchison, 2008). This resulted in sedimentation of various facies both from terrestrial and marine sources (Davies and Kidd, 1977). The ‘soft’ collision between Greater India and Eurasia (Patriat and Achache, 1984; Lee and Lawyer, 1995) resulted in a hiatus manifested as the P unconformity (Curry et al., 1982). This P unconformity is the horizon H4 (Paleocene) in the present study, overlying the pre-fan sediments which thin eastward and were derived from the adjoining landmass (Figure 9c). Further, it is inferred that the pre-fan sediment thickness west of 85ER is up to 3 sec TWT (~5 km), while it is relatively less (<1 sec TWT; <2 km) to its east. These thicknesses differ from the ~4 km maximum thickness of pre-fan sediments proposed along the entire East Coast of India by Curry (1994). Further, this major difference in the sediment thickness can be attributed to the varying crustal ages, east and west of the ridge (Figure 9a).

Hard collision of India with Eurasia resulted in Himalayan uplift by Oligocene time (Replumaz and Tapponnier, 2003) and together with climate change, caused intense erosion of the Himalayas and fan sedimentation at rates around 5-10 cm/kyr (Moore et al., 1974; France-Lanord et al., 1993; Clift et al., 2008). This fan sedimentation is seen in our seismic records as thick sequences having strong parallel reflectors (Figures 3 and 5). Rapid erosion of the Himalayas and Indo-Burma Ranges, caused excessive sedimentation in the Bengal Basin since Pliocene time (Alam et al., 2003). But a major rise (~70 m) in sea level (Haq et al., 1987) may have caused the depocenter to move landward cutting off the sediment source from the fan (Cochran, 1990) and reducing the sedimentation rates to 0.5-2 cm/kyr in the Bengal Fan. In our study, this scenario is seen as the transparent sequence deposited at low rates of <2 cm/kyr above the Pliocene unconformity (Table 3).

During the Late Pleistocene, up to 0.8 sec TWT thick sediments were deposited in the north at high sedimentation rates (>20 cm/kyr) (Figure 8, Table 3). The disposition of the Quaternary subfans suggests migration of the depocenter due to periodic channel avulsions resulting in the formation of a series of overlapping channel-levee deposits (Curry et al., 2003; Bergmann et al., 2019). The presence of turbidites alternating with hemipelagic layers in the Bengal Fan are attributed to the interplay between the external forces such as climate change, sea level fluctuations and tectonics of the catchment areas (Weber and Reilly, 2018).

5.5 Controls on sedimentation pattern

We have examined the Amazon Fan, a large submarine fan in the equatorial Atlantic Ocean to understand its sedimentary history. The Amazon Fan has formed due to long-term terrestrial input and influenced by glacio-eustatic sea level fluctuations, climate change and tectonic activities (Flood et al., 1997). The presence of hemipelagic and calcareous clay deposits in this Fan represents a high sea level stand supported by a multiple channel system, while a single channel-levee system causing deposition of coarse-grained sands indicates a low sea level (Flood et al., 1997; Maslin, 2009). Further, the Amazon fan is inactive in the Holocene and is characterized by hemipelagic sedimentation (Flood et al., 1997). All these observations suggest that the sea level fluctuations exert the maximum influence in designing the architecture and locations of the subfans in the Amazon Fan.

In contrast, the Bengal Fan indicates active growth with turbidite sedimentation in the most recent sea level rise and highstand (Weber, 1997). Hence sea level fluctuations may not be the major controlling factor in fan sedimentation here. The climatic conditions and tectonics of the catchment areas seem to play greater role in the growth of the Bengal Fan (France-Lanord et al., 1993; Clift et al., 2008). Based on ^{10}Be concentrations at recent IODP drill sites in the Bay of Bengal, Lenard et al. (2020) inferred negligible impact of climatic changes on the erosion rates in the Himalayas during the late Cenozoic, implying that tectonics play a bigger role in the fan sedimentation. A study based on paleoproductivity proxies for the last 2.3 Ma at the IODP Leg 353 Site U1445 proposes changes in riverine discharge across the Mid-Pleistocene Transition linked to the global climate change rather than Himalayan uplift (Lee et al., 2020). Isotopic analysis (Sr-Nd) at the same drill site suggests that the Indian summer monsoon rainfall is the major factor controlling the younger sedimentation since 1.8 Ma, while the older sedimentation (1.8 to 6 Ma) is modulated by climatic fluctuations and as well as tectonics associated with the rise of Shillong plateau, development of Indo-Burma wedge, etc (Peketi et al., 2021). Based on isotopic analysis (Sr, Nd, and Pb) at drill site U1443 on the Ninetyeast Ridge in the southern Bay of Bengal, across five climatic intervals from the middle to late Miocene (15.8–9.5 Ma), it is inferred that the climatic fluctuations play a major role in sedimentation and not the Himalayan tectonics (Bretschneider et al., 2020).

Thus, it is clear that there are contrasting views about the role of climate and tectonics of the source areas in the sedimentary history of the Bengal Fan. Hence, additional detailed investigations are needed to isolate their roles in controlling the fan sedimentation. Further, understanding the influence of climate changes and sea level fluctuations on sedimentation may help us to envisage future disastrous events. For a detailed investigation of the Bengal Fan and its Quaternary subfans in

particular, the vertical resolution of the multichannel seismic data appears inadequate. Further, though we see deformation signatures at the continental rise on our profiles, we are unable to make any major inferences. Both these constraints may be overcome by acquiring dense high resolution seismic data, deep well logs and wide-angle refraction data across the Bengal Fan.

6. Conclusions

- Detailed correlation of the recent drill results with multichannel seismic data helped to validate the ages of the major seismic horizons in the Bay of Bengal. Major horizons including three (Paleocene, Pliocene and Late Pleistocene unconformities) were inferred.
- The present study suggests that the 85ER has emplaced during the Middle Cretaceous. Mild folding/faulting is seen on either flank of 85ER up to Pliocene time. The presence of the ridge has influenced the sediment distribution in the study area.
- Older sediments (up to Late Cretaceous time) are thick west of 85ER where the underlying crust is of Early Cretaceous age. East of the 85ER, these sediments are thin probably due to its younger (Middle Cretaceous) crustal age.
- Sediments up to Paleocene time thin eastward, implying that they are derived from the adjoining landmass. Thereafter, a change in sedimentation to the fan type is manifested as a prominent unconformity H4. Fan sedimentation is seen as strong, continuous, parallel reflections, overlapping onto older horizons along the continental slope.

The present study facilitated the identification of U_g as Late Pleistocene and U_h as Pliocene unconformities along 17°N (Schwenk and Spiess, 2009). Further the discrepancies between the subfans identified by Curry et al. (2003) and Bergmann et al. (2019) could be resolved. Our seismic network aided to infer the western extents of the subfans A to D in the study area.

- The transparent sequence between the Late Pleistocene and Pliocene unconformities is seen nearly throughout the study area and is thinner on the 85ER.
- The study generated a revised seismic stratigraphy of the northwestern Bay of Bengal. The inferences drawn from this study provide important constraints for its sedimentary history. These results can serve as an updated base for future investigations in the northwestern Bay of Bengal.

Data statement

The seismic data are provided by the Directorate General of Hydrocarbons (DGH, Ministry of Petroleum & Natural Gas, Government of India). The data may be obtained from DGH on submission of a suitable research proposal.

Acknowledgements

Director, NIO is thanked for granting the necessary permission. We are grateful to Directorate General of Hydrocarbons (DGH), India for providing the seismic data. Figures are generated using GMT software (Wessel and Smith, 1998). We thank Dr. W. H. Geissler and two anonymous reviewers for their constructive comments. This is CSIR-NIO contribution

References

- Alam, M., Alam, M., Curray, J.R., Chowdhury, M.L.R., Gani, M.R., 2003. An overview of the sedimentary geology of the Bengal basin in relation to the regional tectonic framework and basin-fill history. *Sed. Geology* 155, 179–208.
- Ali, J.R., Aitchison, J.C., 2008. Gondwana to Asia: Plate tectonics, paleogeography and the biological connectivity of the Indian sub-continent from the Middle Jurassic through latest Eocene (166-35 Ma). *Earth Sci. Rev.*, 88, 145-166.
- Altenbernd, T., Jokat, W., Geissler, W., 2020. The bent prolongation of the 85°E Ridge south of 5°N – Fact or fiction? *Tectonophysics* <https://doi.org/10.1016/j.tecto.2020.228457>.
- Bastia, R., Radhakrishna, M., Srinivas, T., Nayak, S., Nathaniel, D.M., Biswal, T.K., 2010. Structural and tectonic interpretation of geophysical data along the Eastern Continental Margin of India with special reference to the deep water petroliferous basins. *J. Asian Earth Sci.* 39, 608–619.
- Bergmann, F., Schwenk, T., Spiess, V., France-Lanord, C., 2020. Middle to Late Pleistocene Architecture and Stratigraphy of the lower Bengal Fan—Integrating multichannel seismic data and IODP Expedition 354 results. *Geochem. Geophys. Geosys.* 21, e2019GC008702. [doi:10.1029/2019GC008702](https://doi.org/10.1029/2019GC008702)
- Bouma, A. (2001). Fine-grained submarine fans as possible recorders of long-and short-term climatic changes. *Global and Planetary Change*, 28(1), 85-91. [doi:10.1016/S0921-8181\(00\)00066-7](https://doi.org/10.1016/S0921-8181(00)00066-7)
- Bretschneider, L., Hathorne, E. C., Huang H., Lübbers, J., Kochhann, K. G. D., Holbourn, A., Kuhnt, W., Thiede, R., Gebregiorgis, D., Giosan, L., Frank, M., 2020. Provenance and Weathering of Clays Delivered to the Bay of Bengal During the Middle Miocene: Linkages to Tectonics and Monsoonal Climate. *Paleocean. Paleoclimat.*, 36, e2020PA003917. [doi:10.1029/2020PA003917](https://doi.org/10.1029/2020PA003917)

- Choudhuri, M., Nemcok, M., Stuart, C., Welker, C., Sinha, S.T., Bird, D., 2014. 85°E Ridge, India – Constraints on its Development and Architecture. *J. Geol. Soc. India*, 84, 513-530.
- Choudhuri, M., Nemcok, M., Melichar, R., Sinha, N., 2017. Propagation of hotspot volcanism driven flexure in oceanic crust -85°E Ridge case study. *Mar. Pet. Geol.* 82, 134-153.
- Clemens, S.C., et al., 2016. Site U1444. *Proc. IODP*, Vol. 353, College Station, TX. doi:10.14379/iodp.proc.353.104.
- Clift, P. D., Hodges, K. V., Heslop, D., Hannigan, R., Van Long, H., Calves, G., 2008. Correlation of Himalayan exhumation rates and Asian monsoon intensity. *Nature Geosc.* 1(12), 875–880.
- Cochran, J.R., 1990. Himalayan uplift, sea level, and the record of Bengal fan sedimentation at the ODP Leg 116 sites. In: Cochran J.R. et al., (Eds.), *Proc. ODP, Sci. Res. 116*, pp. 397-414.
- Crosby, A.G., Mckenzie, D., Sclater, J.G., 2006. The relationship between depth, age and gravity in the oceans. *Geophys. J. Int.*, 166, 553-573.
- Curry, J. R., 1994. Sediment volume and mass beneath the Bay of Bengal. *Earth Planet. Sci. Lett.* 125, 371-383.
- Curry, J. R., Emmel, F. J., Moore, D. G., Raitt, R. W., 1982. Structure, tectonics and geological history of the Northeastern Indian Ocean. In: Nairn, A. E., Stehli, F. G. (Eds.) *The Ocean Basins and Margins 6*, Plenum, New York, pp. 399-450.
- Curry, J.R., Moore, D.G., 1971. Growth of the Bengal deep-sea fan and denudation in the Himalayas. *Geol. Soc. Am.* 82, 563–572.
- Curry, J. R., Moore, D. G., 1974. Sedimentary and tectonic processes in the Bengal Deep Sea Fan and Geosyncline. In: Burk, C. A., Drake, C. L. (Eds.) *Continental Margins* New York, Springer-Verlag, pp. 617-627.
- Curry, J. R., Munasinghe, T., 1989. Timing of intraplate deformation, northeastern Indian Ocean. *Earth Planet. Sci. Lett.* 94, 71-77.
- Curry, J. R., Munasinghe, T., 1991. Origin of the Rajmahal Traps and the 85°E Ridge: Preliminary reconstructions of the Crozet hotspot. *Geology* 19, 1237-1240.
- Curry, J. R., Emmel, F. J., Moore, D. G., 2003. The Bengal Fan: morphology, geometry, stratigraphy, history and processes. *Mar. Petr. Geol.* 19, 1191-1223.
- Dangwal, V., Sengupta, S., Desai, A.G., 2008. Speculated Petroleum Systems in Deep Offshore Mahanadi Basin in Bay of Bengal, India. 7th Int. Conf. & Expo. Petr. Geophys. Hyderabad, 2008.
- Davies, T.A., Kidd, R. B., 1977. Sedimentation in the Indian Ocean through time. In: Heirtzler, J.R. et al., (Eds.) *Indian Ocean geology and biostratigraphy*. AGU, pp. 61-86.
- Depluse, C., Diament, M., Hébert, H., Bertrand, G., Dominguez, S., Dubois, J., Malod, J., Patriat, P., Pontoise, B., Sibilla, J.J., 1998. Direct evidence of active deformation in the eastern Indian Oceanic plate. *Geology* 26, 131-134.

- Desa, M., Ramana, M. V. Ramprasad, T., Lall, M. V., Kumar, B.J.P., 2013. Geophysical signatures over and around the northern segment of the 85°E Ridge, Mahanadi offshore, Eastern Continental margin of India: Tectonic implications. *J. Asian Earth Sci.* 73, 460-472.
- Desa, M., Ramana, M. V., 2016. Middle Cretaceous geomagnetic field anomalies in the Eastern Indian Ocean and their implication to the tectonic evolution of the Bay of Bengal, *Mar. Geol.* 382, 111–121.
- Duncan, R.A., 1991. Age distribution of volcanism along aseismic ridges in the eastern Indian Ocean. In: Weissel, J; Peirce, J; Taylor, E; et al. (Eds.), *Proceedings of the Ocean Drilling Program, Scientific Results*, College Station, TX (Ocean Drilling Program), 121, 507-517, [doi:10.2973/odp.proc.sr.121.162.1991](https://doi.org/10.2973/odp.proc.sr.121.162.1991)
- Flood, R. D., Piper, D. J.W., Klaus, A., Peterson, L.C. 1997. *Proceedings of the Ocean Drilling Program, Sci. Res.*, 155, College Station, Texas, Ocean Drilling Program, 1233 pp.
- France-Lanord, C., Derry, L., Michard, A., 1993. Evolution of the Himalaya since Miocene time: Isotopic and sedimentological evidence from the Bengal Fan. *Geol. Soc. London Sp. Pub.* 74 (1), 603–621.
- France-Lanord, C., Spiess, V., Schwenk, T., Klaus, A., Scientists, Exp. 354, 2016. *Proc. IODP*, 354, College Station, TX, [doi:10.14379/iodp.proc.354.2016](https://doi.org/10.14379/iodp.proc.354.2016)
- Geller, C.A., Weissel, J.K., Anderson, R.N., 1983. Heat transfer and intraplate deformation in the central Indian Ocean. *J. Geophys. Res.* 88, 5560-5570.
- Gopala Rao, D., Bhattacharya, GC, Ramana, MV, Krishna, K.S., et al., 1994. Analysis of multi-channel seismic reflection and magnetic data along 13°N latitude across the Bay of Bengal. *Mar. Geophys. Res.* 16, 225-236.
- Gopala Rao, D., Krishna, K.S., Sar, D., 1997. Crustal evolution and sedimentation history of the Bay of Bengal since the Cretaceous. *J. Geophys. Res.* 102, 17747-17768.
- Gorain S., Sachdeva, H., 2017. *Mystery beneath the 85°E Ridge*, SPG-India, Jaipur 2017.
- Gordon, R.G., DeMets, C., Royer, J-Y., 1998. Evidence for long-term diffuse deformation of the lithosphere of the equatorial Indian Ocean. *Nature* 395, 370-373.
- Gradstein, F. M., Ogg, J. G., Schmitz, M. D., Ogg, G. M., 2012. *The Geologic Time Scale 2012*, 2, Elsevier, Boston, 1176 pp. plus chart.
- Haq, B.U., Hardenbol, J., Vail, P.R. 1987. Chronology of the fluctuating sea levels since the Triassic. *Science*, 235, 1156-1167.
- Heezen, B.C., Tharp, M., 1964. *Physiographic Diagram of the Indian Ocean (With Descriptive Sheet)*. Geological Society of America, New York.
- Kent, R., 1991. Lithospheric uplift in eastern Gondwana: Evidence for a long-lived mantle plume system? *Geology* 19, 19–23.

- Kent, R. W., Storey, M., Saunders, A. D., Ghose, N. C., Kempton, P. D., 1992. Comments and reply on "Origin of the Rajmahal Traps and the 85°E Ridge: Preliminary reconstructions of the trace of the Crozet hotspot. *Geology* 20, 957-958.
- Krishna, K.S., Bull., J.M., Scrutton, R.A., 2001. Evidence for multiphase folding of the Central Indian Ocean lithosphere. *Geology* 29, 715-718.
- Krishna, K.S., 2003. Structure and evolution of the Afanasy Nikitin seamount, buried hills and 85°E Ridge in the northeastern Indian Ocean. *Earth Planet. Sci. Lett.* 209, 379–394. doi:10.1016/S0012-821X(03)00081-5.
- Krishna, K.S., Ismaiel, M., Srinivas, K., Gopala Rao, D., Mishra, J., Saha, D., 2016. Sediment pathways and emergence of Himalayan source material in the Bay of Bengal. *Curr. Sci.* 110, 1-12.
- Lee, T-Y, Lawver, L. A., 1995. Cenozoic plate reconstruction of Southeast Asia. *Tectonophysics* 251, 85-138.
- Lee, J., Kim, S., Khim, B-K., 2020. A paleoproductivity shift in the northwestern Bay of Bengal (IODP Site U1445) across the Mid-Pleistocene transition in response to weakening of the Indian summer monsoon. *Palaeogeog. Palaeoclim., Palaeoecol.*, 560, 110018.
- Lenard, S.J.P., Lave, J., France-Lanord, C., Aumaitre, G., Bourles, D.L., Keddadouche, K., 2020. Steady erosion rates in the Himalayas through late Cenozoic climatic changes. *Nature Geosci.*, doi:10.1038/s41561-020-0585-2
- Liu, C., Sandwell, D.T., Curray, J.R., 1982. The Negative Gravity Field over the 85°E Ridge. *J. Geophys. Res.* 87, 7673–7686. doi:10.1029/JB087iB09p07673.
- Maslin, M.A., 2009. Review of the timing and causes of the Amazon-Fan mass transport and avulsion deposits during the latest Pleistocene. In: *External Controls on deep-water depositional systems*. SEPM Sp. Pub. 92, 133-144.
- Matthews, K.J., Seton, M., Muller, R.D., 2012. A global-scale plate reorganization event at 105-100 Ma. *Earth Planet. Sci. Lett.* 355-356, 283-298.
- Michael, L., Krishna, K.S., 2011. Dating of the 85°E Ridge (northeastern Indian Ocean) using marine magnetic anomalies. *Curr. Sci.* 100, 1314-1322.
- Moore, D. G., Curray, J. R., Raitt, R. W., Emmel, F. J., 1974, Stratigraphic-seismic section correlations and implications to Bengal Fan history. In: C. C. von der Borch, J. G. Sclater et al.,(Eds.) Washington, D. C., U. S. Gov. Printing Office, pp. 403-412.
- Muller, R.D., Yatheesh, V., Shuhail, M., 2015. The tectonic stress field evolution of India since the Oligocene. *Gondwana Research*, 28, 612-624.
- Nayak, S., Das, S., Bastia, R., Kar, B., 2011. Petroleum System Related to 85° E Ridge: A Conceptual Study. Search and Discovery article #50497, AAPG, 2011.
- Patriat, P., Achache, J., 1984. India–Eurasia collision chronology has implications for crustal shortening and driving mechanism of plates. *Nature* 311, 615-621.

- Peketi, A., Mazumdar, A., Pillutla, S.P.K., Sawant, B., Gupta, H., 2021. Climatic and tectonic control on the Bengal Fan sedimentation since the Pliocene. *Geochem. Geophys. Geosys.*, 22, doi:10.1029/2020GC009448
- Powell, C. M., Roots, S. R., Veevers, J. J., 1988. Pre-breakup continental extension in East Gondwanaland and the early opening of the eastern Indian Ocean. *Tectonophysics* 155, 261-283.
- Ramana, M. V., Nair, R. R., Sarma, K. V. L. N. S., Ramprasad, T., Krishna, K. S., Subrahmanyam, V., D'Cruz, M., Subrahmanyam, C., Paul, J., Subrahmanyam, A. S., Chandrasekhar, D. V., 1994. Mesozoic anomalies in the Bay of Bengal. *Earth Planet. Sci. Lett.* 121, 469 - 475.
- Ramana, M. V., Subrahmanyam, V., Chaubey, A.K., Ramprasad, T., Sarma, K. V. L. N. S., Krishna, K. S., Desa, M., Murty, G.P.S., 1997. Structure and origin of the 85°E Ridge. *J. Geophys. Res.* 102, 17995-18012.
- Rao, G.N. 2001. Sedimentation, Stratigraphy, and Petroleum Potential of Krishna-Godavari Basin, East Coast of India. *Am. Ass. Pet. Geol.* 85, 1623-1643.
- Replumaz, A., Tapponnier, P., 2003. Reconstruction of the deformed collision zone between India and Asia by backward motion of lithospheric blocks. *J. Geophys. Res.* 108, doi:10.1029/2001JB000661
- Royer, J-Y, Sandwell, D.T., 1989. Evolution of the Eastern Indian Ocean since the Late Cretaceous: Constraints from Geosat altimetry. *J. Geophys. Res.* 94, 755 782.
- Sandwell, D.T., Muller, R. D., Smith, W. H. F., Garcia, E., Francis, R., 2014. New global marine gravity model from CryoSat-2 and Jason-1 reveals buried tectonic structure. *Science* 346, 65-67.
- Schwenk, T., Spiess, V., 2009. Architecture and stratigraphy of the Bengal Fan as response to tectonic and climate revealed from high-resolution seismic data. *External Controls on Deep-Water Depositional Systems SEPM Special Publication No. 92*, SEPM (Society for Sedimentary Geology), ISBN 978-1-56576-200-8, pp. 107–131.
- Shanmugam, G., Muiola, R.J., 1982. Eustatic control of turbidites and winnowed turbidites. *Geology* 10, 231-235.
- Siawal, A., Radhakishan, Rawat, C.P.S., Prakash, R., Saha, D., Parakh, A.K., 2015. Significant Geophysical signatures in Bay of Bengal and geological model of emplacement of 85°E Ridge. 11th Biennial Int. Conf & Expo., Jaipur, SPG-India.
- Smith, W. H. F., Sandwell, D., 1997. Global seafloor topography from satellite altimetry and ship depth soundings. *Science* 277, 1956-1962.
- Talwani, M., Desa, M. A., Ismaiel, M., Krishna, K.S., 2016. The Tectonic Origin of the Bay of Bengal and Bangladesh. *J. Geophys. Res.* 121, 4836–4851, doi:10.1002/2015JB012734.
- Von der Borch, C.C., Sclater, J.G., et al., 1974. Initial Reports, DSDP22, Washington (US Govt. Printing Office), 885 pp.

- Weber, M.E., Wiedicke, M.H., Kudrass, H.R., Hubscher, C., Erlenkeuser, H., 1997. Active growth of the Bengal Fan during sea-level rise and highstand. *Geology* 25, 315-318.
- Weber, M. E., Reilly, B. T., 2018. Hemipelagic and turbiditic deposits constrain lower Bengal Fan depositional history through Pleistocene climate, monsoon, and sea level transitions. *Quat. Sci. Rev.*, 199, 159–173. [doi:10.1016/j.quascirev.2018.09.027](https://doi.org/10.1016/j.quascirev.2018.09.027)
- Weissel, J.K., Anderson, R.N., Geller, C.A., 1980. Deformation of the Indo-Australian plate. *Nature* 287, 284-291.
- Wessel, P. Smith, W. H. F., 1998. New improved version of Generic Mapping Tools released. *EOS Trans., Amer. Geophys. Un.* 79, 579.
- Wessel, P., Matthews, K.J., Muller, R.D., Mazzoni, A., Whittaker, J.M., Myhill, R., Chandler, M.T., 2015. Semi automatic fracture zone tracking. *Geochem. Geophys. Geosyst.* doi: 10.1002/2015GC005853.
- Wiens, D.A., DeMets, C., Gordon, R.G., Stein, S., Argus, D., Engeln, J.F., Lundgren, P., Quible, D., Stein, C., Weinstein, S., Woods, D.F., 1985. A diffuse plate boundary model for Indian Ocean tectonics. *Geophys. Res. Lett.* 12, 429-432.

Figure Captions

Figure 1: Gravity picture of the Bay of Bengal (Sandwell et al., 2014). Ninetyeast (NER) and 85°E Ridges (85ER) are indicated. Fracture zones are marked as blue dashed lines (Wessel et al., 2015). The northern extent of deformation is shown as a red outline (Gordon et al., 1998). Study area is shown as a white box. Continent-Ocean Transition is marked in pink. 86EFZ: 86°E Fracture Zone; ANS: Afanasy Nikitin Seamount chain; AS: Andaman Sea; CR: Comorin Ridge; K-G: Krishna-Godavari; SL: Sri Lanka; ST: Sunda Trench.

Figure 2: Bathymetry map of the Bay of Bengal (Smith and Sandwell, 1997) overlain by the seismic tracks. GXT tracks are in red and published east-west lines are in black (Gopala Rao et al., 1994; Gopala Rao et al., 1997; Michael and Krishna, 2011). Tracks of Schwenk and Spiess (2009) are in yellow, while tracks of Curray et al. (2003) are in orange. Tracks whose seismic record is displayed are thickened and figure numbers are provided. Drill sites used in this study are marked as black circles. Gravity low of the 85ER is marked in cyan. Small black squares represent DSDP/IODP drill sites. Acronyms as in figure 1.

Figure 3: Interpreted seismic record of the profile GXT1290. Locations of drill sites K-1 and AA with lithology are indicated. Well-seismic correlation details are given in figure S3. Horizons (H1 to H9) identified based on the drill sites are marked in different colours. Location of the profile is shown in figure 2. Tie point with GXT4000 is marked. Faults are marked as black dashed lines. 85ER represents the 85°E Ridge.

Figure 4: Composite figure depicting a seismic window of GeoB97-041 (Schwenk and Spiess, 2009) along with U1444 drill site superimposed on SK107-07 seismic record. Small seismic windows of GXT1100 and GXT1200 are placed at their tie points with SK107-07. This exercise helped in transferring the U_c and U_d unconformities from U1444 to our seismic network.

Figure 5: Interpreted seismic records depicting the horizons identified along the seismic profile GXT4000. Location of the profile is shown in figure 2. Tie points with other GXT profiles are also marked. 85ER represents the 85°E Ridge. Remaining information as in Figure 3.

Figure 6: Composite figure depicting the seismic record along GXT1800 and the eastern segment of GeoB97-059/069 (Schwenk and Spiess, 2009). Location of the profiles is shown in figure 2. Correlation of the horizons suggests that U_g and U_h are Late Pleistocene (H9) and Pliocene (H8) unconformities respectively. The tie points of Curray et al. (2003) profiles at 19.4°N and 19°N with GXT1800 are indicated as C19.4n and C19n respectively. Subfans A, B and D (red labels) are marked from Curray et al. (2003), while subfans B to D (black labels) are marked from Bergmann et al. (2019).

Figure 7: Seismic record along GXT1240 depicting the 85ER and the sediment load. Faulting and folding is seen at the western edge of the 85ER. Multiple faulting episodes can be inferred as indicated by arrows. A sedimentary wedge is seen west of the fault (below green arrow). The sediments between horizons H8 and H9 are transparent similar to those inferred by Schwenk and Spiess (2009). Subfan B onlaps onto H9 and wedges out towards east. The location of the record is provided in figure 2.

Figure 8: Late Pleistocene sediment isopach map of the study area (Interval is 0.05 sec TWT). Sediment thickness is more than 0.6 sec TWT in the northeast, while it is as low as 0.1 sec TWT around 85ER (outlined in cyan). In the southeast, the 0.4 sec TWT thick sediments are seen off Krishna-Godavari (K-G). The western extents of the subfans are shown as red (subfan A), green (subfan B), blue (subfan C) and pink (subfan D) outlines. These extents are in agreement with those proposed by Curray et al. (2003) and Bergmann et al. (2019).

Figure 9

(a) Crustal age distribution map of the Bay of Bengal (modified from Desa and Ramana, 2016). The crustal age is maximum (up to 132 Ma) off the central East Coast of India and decreases towards south and east. A north-south trend is seen along the eastern edge of the gravity low (marked in white) attributed to the 85ER. SL: Sri Lanka

(b) Basement depths in sec TWT at 100 Ma computed using the formula given in Crosby et al. (2006) (computation details given in supplementary information). Basement depths are in the range of 3.8 to 6.0 sec TWT. The relief of 85ER at this time is superimposed in red contours with an interval of 0.5 sec TWT. The figure depicts that the 85ER was subaerial with a maximum relief of 2 sec TWT around 14°N. SL: Sri Lanka

(c) Basement depths in sec TWT at 58 Ma, computed as above. Basement depths are in the range of 5.8 to 7.5 sec TWT. Pre-fan sediment isopachs are superimposed in red with an interval of 0.5 sec TWT. Pre-fan sediment thickness ranges from >2 sec TWT off the East Coast to 1 sec TWT in the northeast. Clustering of the isopachs around 85ER depicts the influence of the ridge on sedimentation. SL: Sri Lanka

List of Tables

Table 1: Subsurface lithology and ages at drill site K-1 and the corresponding horizons along the seismic record GXT1290 (modified from Krishna et al., 2016). Interval velocities are from the well logs, while the sedimentation rates are calculated after decompaction of the layers as provided in the supplementary information. The geological ages are from Gradstein et al. (2012).

Table 2: Subsurface lithology and ages at drill site AA and the corresponding horizons along the seismic record GXT1290. Remaining information as in table 1.

Table 3: Subsurface lithology and ages at drill site U1444 and the corresponding horizons along the seismic record GeoB97-041. Remaining information as in table 1.

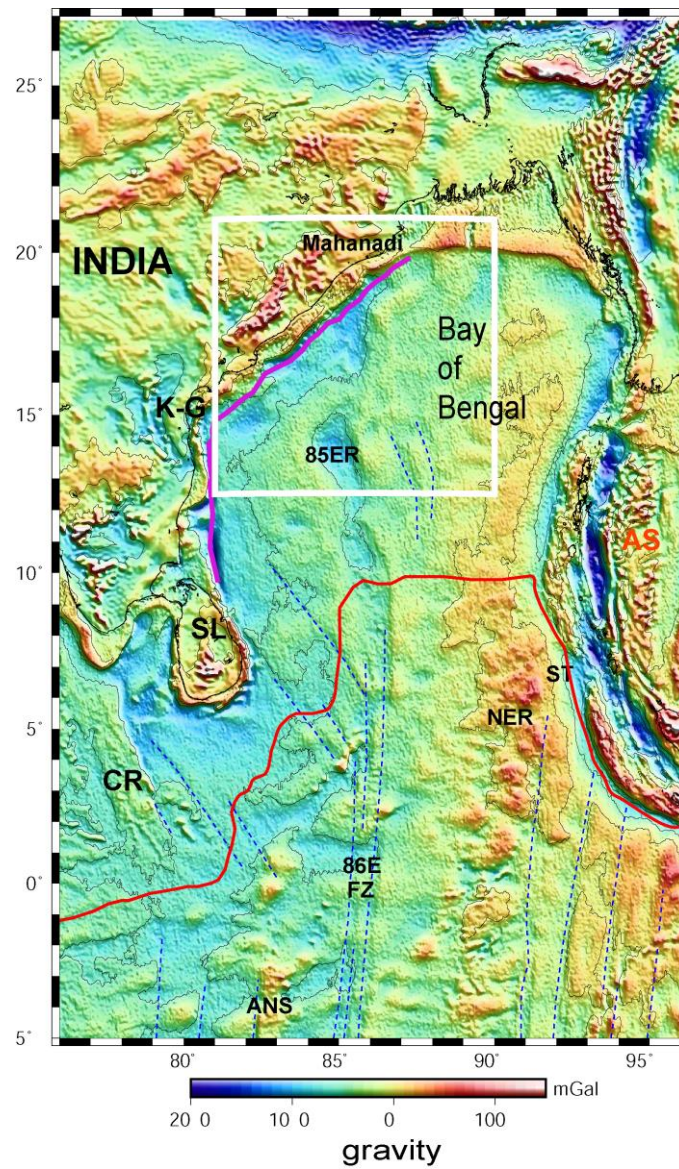


Figure 1

Figure 1: Gravity picture of the Bay of Bengal (Sandwell et al., 2014). Ninetyeast (NER) and 85°E Ridges (85ER) are indicated. Fracture zones are marked as blue dashed lines (Wessel et al., 2015). The northern extent of deformation is shown as a red outline (Gordon et al., 1998). Study area is shown as a white box. Continent-Ocean Transition is marked in pink. 86EFZ: 86°E Fracture Zone; ANS: Afanasy Nikitin Seamount chain; AS: Andaman Sea; CR: Comorin Ridge; K-G: Krishna-Godavari; SL: Sri Lanka; ST: Sunda Trench.

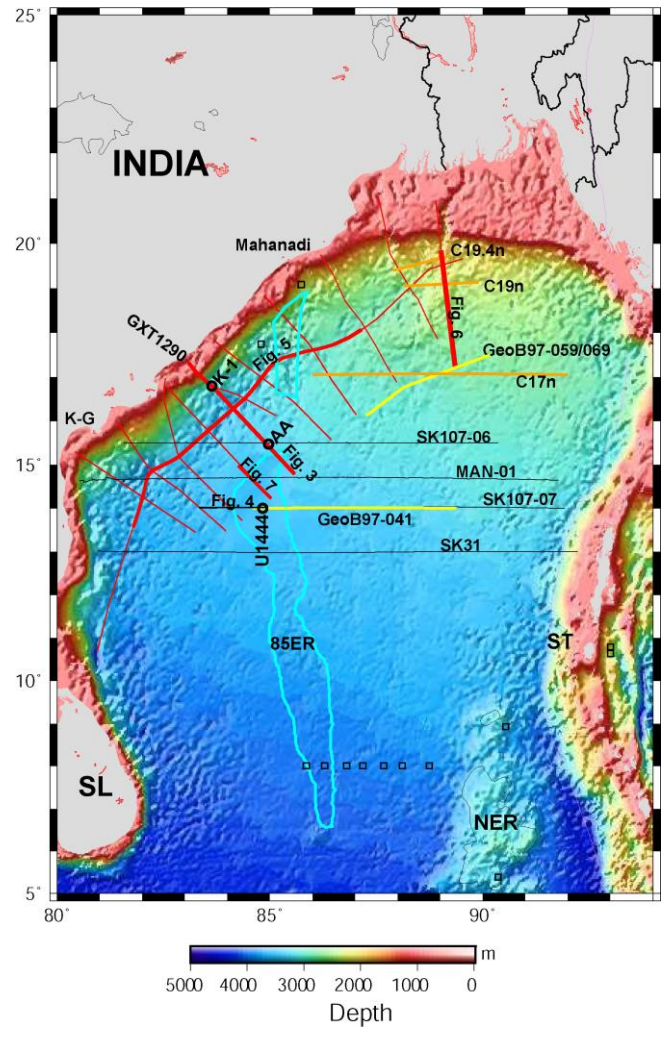


Figure 2

Figure 2: Bathymetry map of the Bay of Bengal (Smith and Sandwell, 1997) overlain by the seismic tracks. GXT tracks are in red and published east-west lines are in black (Gopala Rao et al., 1994; Gopala Rao et al., 1997; Michael and Krishna, 2011). Tracks of Schwenk and Spiess (2009) are in yellow, while tracks of Curry et al. (2003) are in orange. Tracks whose seismic record is displayed are thickened and figure numbers are provided. Drill sites used in this study are marked as black circles. Gravity low of the 85ER is marked in cyan. Small black squares represent DSDP/IODP drill sites. Acronyms as in figure 1.

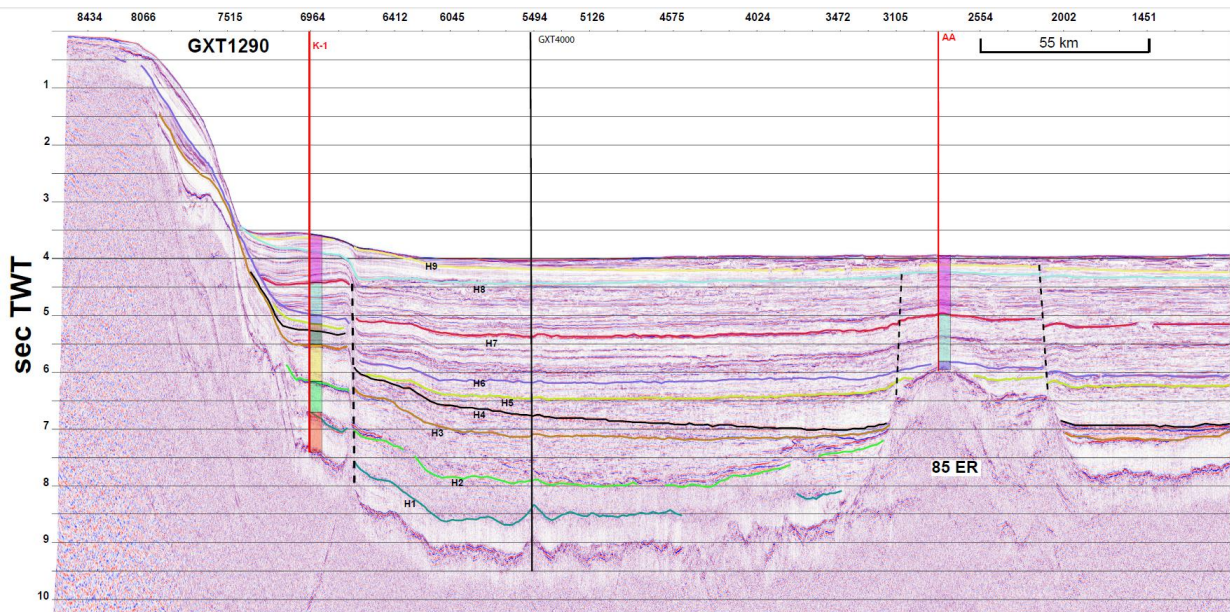


Figure 3

Figure 3: Interpreted seismic record of the profile GXT1290. Locations of drill sites K-1 and AA with lithology are indicated. Well-seismic correlation details are given in figure S3. Horizons (H1 to H9) identified based on the drill sites are marked in different colours. Location of the profile is shown in figure 2. Tie point with GXT4000 is marked. Faults are marked as black dashed lines. 85ER represents the 85°E Ridge.

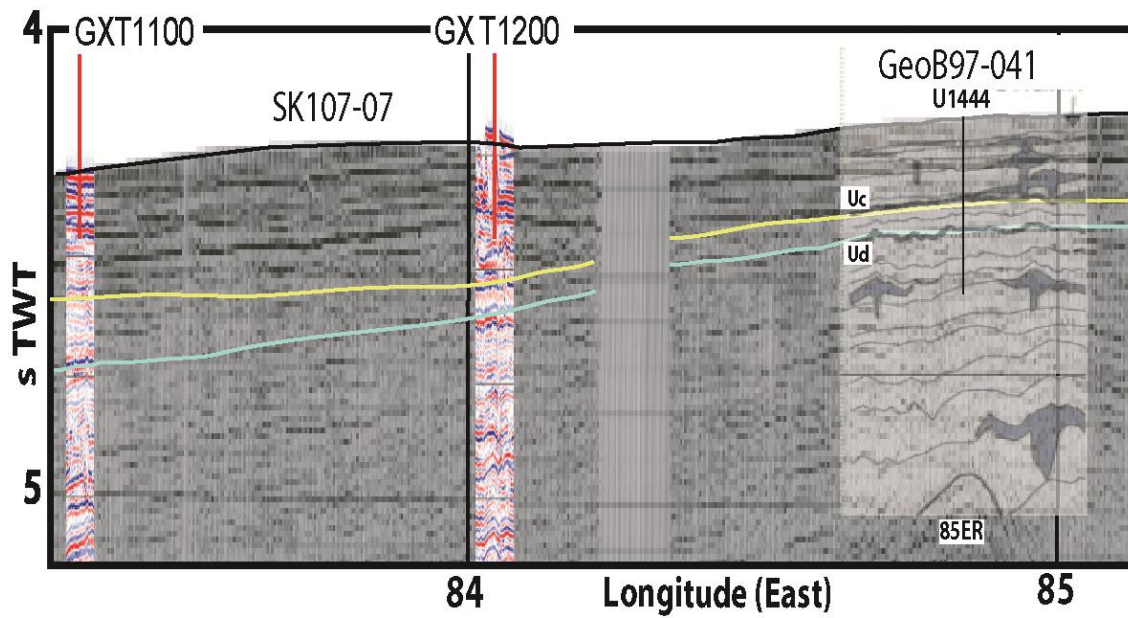


Figure 4

Figure 4: Composite figure depicting a seismic window of GeoB97-041 (Schwenk and Spiess, 2009) along with U1444 drill site superimposed on SK107-07 seismic record. Small seismic windows of GXT1100 and GXT1200 are placed at their tie points with SK107-07. This exercise helped in transferring the U_c and U_d unconformities from U1444 to our seismic network.

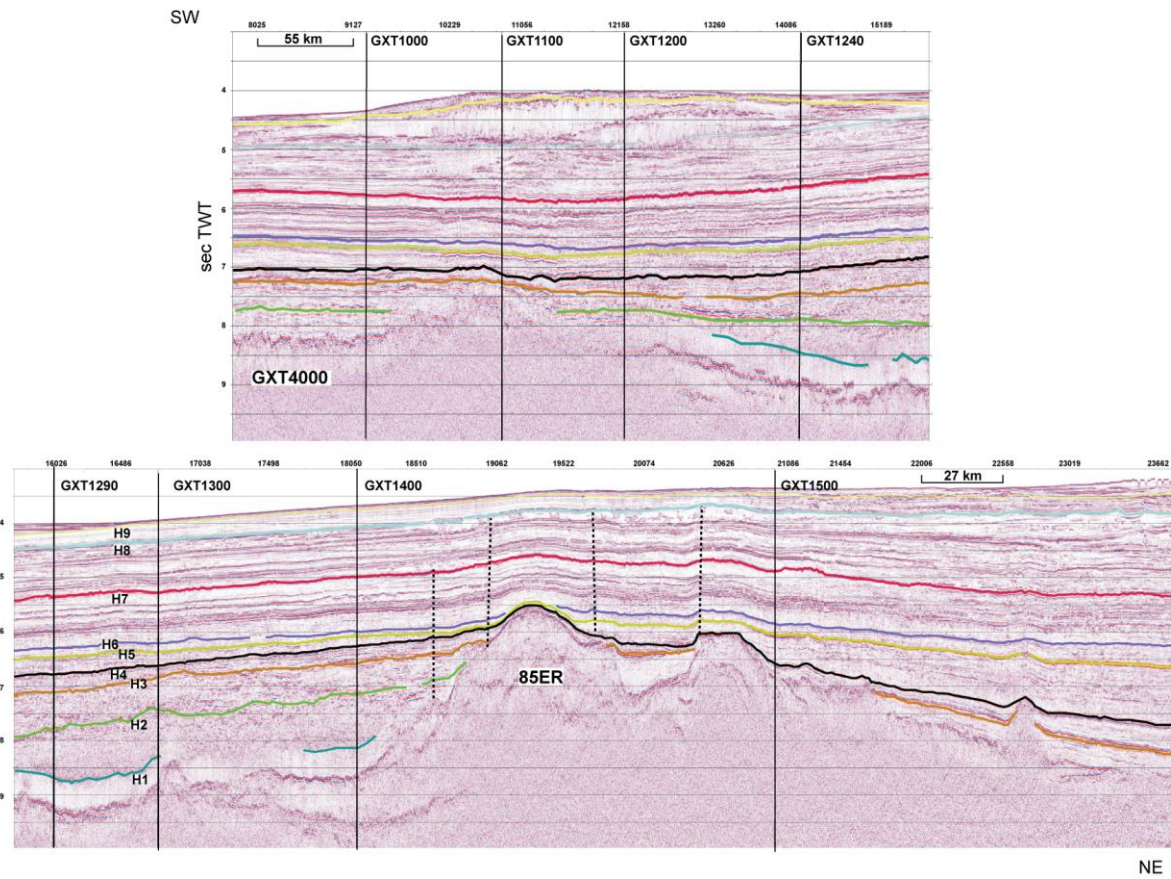


Figure 5

Figure 5: Interpreted seismic records depicting the horizons identified along the seismic profile GXT4000. Location of the profile is shown in figure 2. Tie points with other GXT profiles are also marked. 85ER represents the 85°E Ridge. Remaining information as in Figure 3.

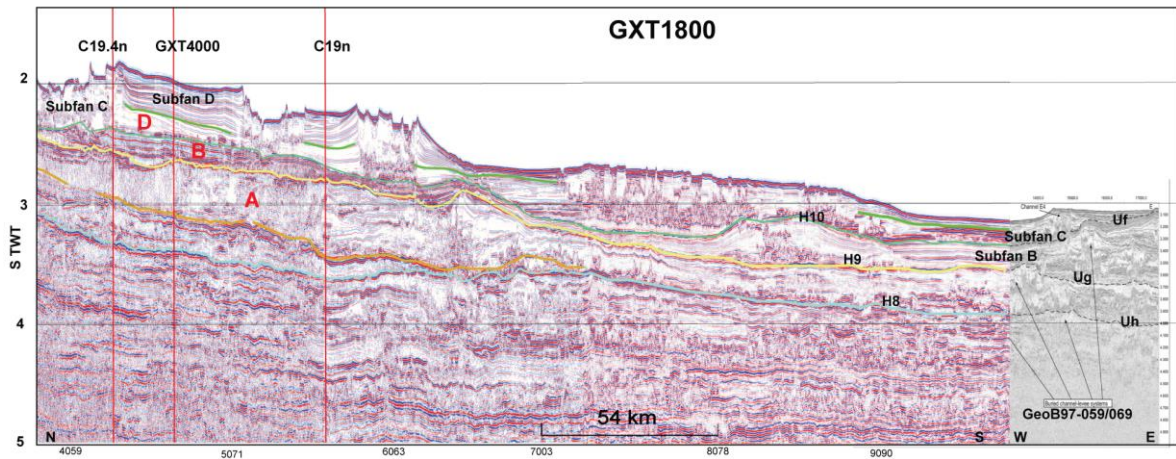


Figure 6

Figure 6: Composite figure depicting the seismic record along GXT1800 and the eastern segment of GeoB97-059/069 (Schwenk and Spiess, 2009). Location of the profiles is shown in figure 2. Correlation of the horizons suggests that U_g and U_h are Late Pleistocene (H9) and Pliocene (H8) unconformities respectively. The tie points of Curray et al. (2003) profiles at 19.4°N and 19°N with GXT1800 are indicated as C19.4n and C19n respectively. Subfans A, B and D (red labels) are marked from Curray et al. (2003), while subfans B to D (black labels) are marked from Bergmann et al. (2019).

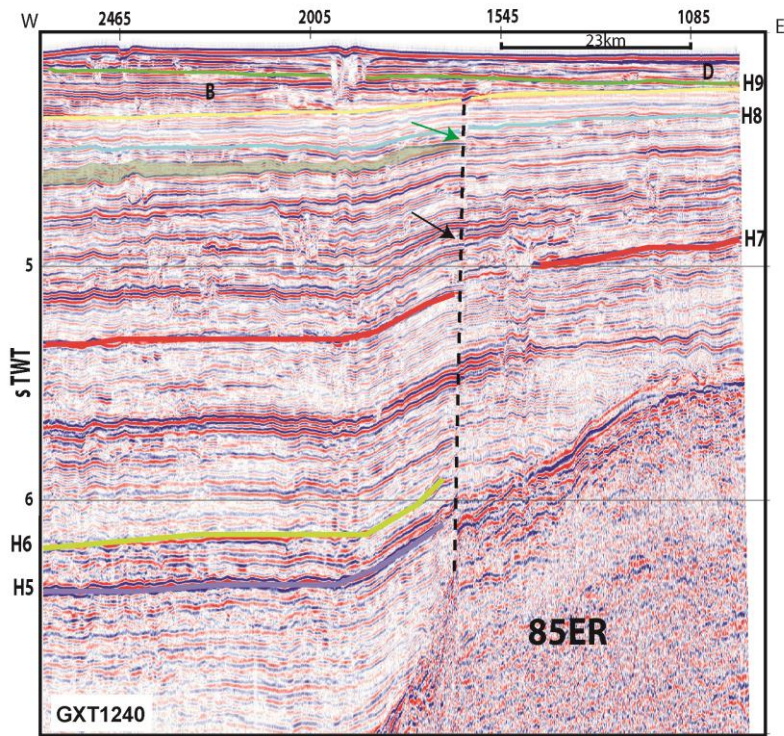


Figure 7

Figure 7: Seismic record along GXT1240 depicting the 85ER and the sediment load. Faulting and folding is seen at the western edge of the 85ER. Multiple faulting episodes can be inferred as indicated by arrows. A sedimentary wedge is seen west of the fault (below green arrow). The sediments between horizons H8 and H9 are transparent similar to those inferred by Schwenk and Spiess (2009). Subfan B onlaps onto H9 and wedges out towards east. The location of the record is provided in figure 2.

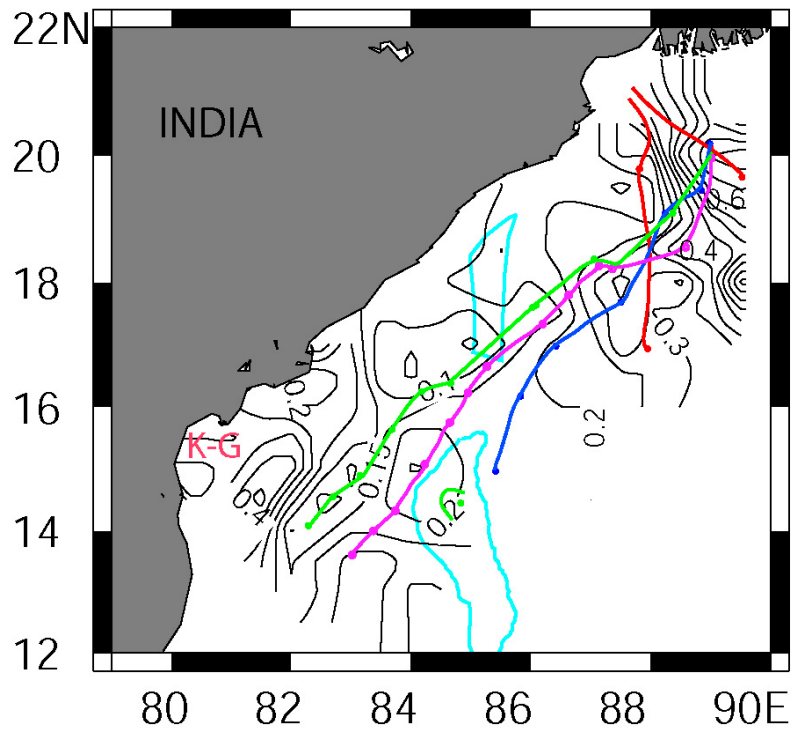


Figure 8

Figure 8: Late Pleistocene sediment isopach map of the study area (Interval is 0.05 sec TWT). Sediment thickness is more than 0.6 sec TWT in the northeast, while it is as low as 0.1 sec TWT around 85ER (outlined in cyan). In the southeast, the 0.4 sec TWT thick sediments are seen off Krishna-Godavari (K-G). The western extents of the subfans are shown as red (subfan A), green (subfan B), blue (subfan C) and pink (subfan D) outlines. These extents are in agreement with those proposed by Curray et al. (2003) and Bergmann et al. (2019).

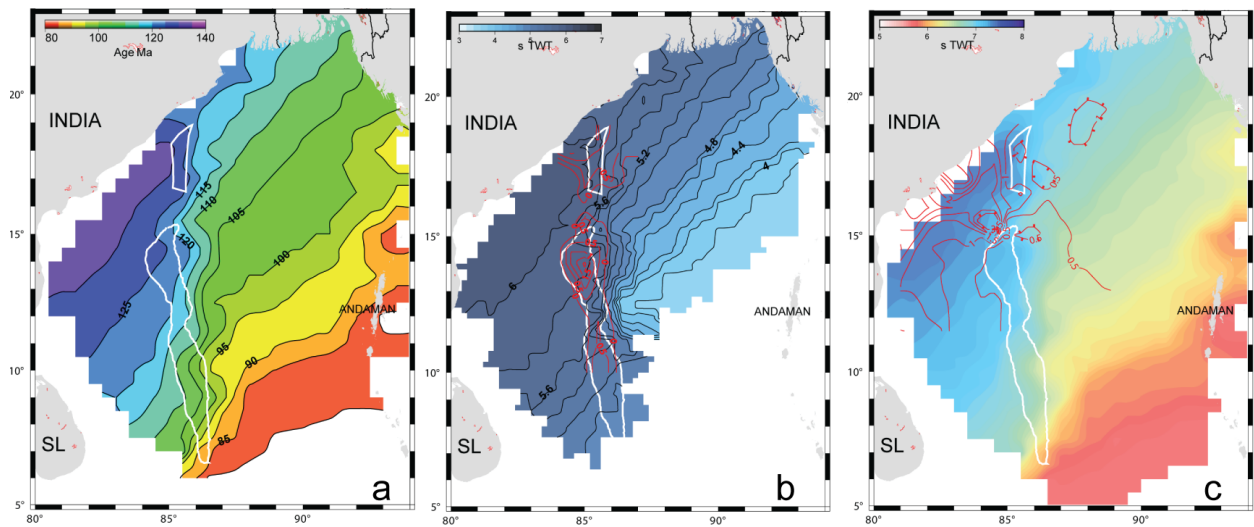


Figure 9

Figure 9: (a) Crustal age distribution map of the Bay of Bengal (modified from Desa and Ramana, 2016). The crustal age is maximum (up to 132 Ma) off the central East Coast of India and decreases towards south and east. A north-south trend is seen along the eastern edge of the gravity low (marked in white) attributed to the 85ER. SL: Sri Lanka

(b) Basement depths in sec TWT at 100 Ma computed using the formula given in Crosby et al. (2006) (computation details given in supplementary information). Basement depths are in the range of 3.8 to 6.0 sec TWT. The relief of 85ER at this time is superimposed in red contours with an interval of 0.5 sec TWT. The figure depicts that the 85ER was subaerial with a maximum relief of 2 sec TWT around 14°N. SL: Sri Lanka

(c) Basement depths in sec TWT at 58 Ma, computed as above. Basement depths are in the range of 5.8 to 7.5 sec TWT. Pre-fan sediment isopachs are superimposed in red with an interval of 0.5 sec TWT. Pre-fan sediment thickness ranges from >2 sec TWT off the East Coast to 1 sec TWT in the northeast. Clustering of the isopachs around 85ER depicts the influence of the ridge on sedimentation. SL: Sri Lanka

Horizon	Lithology and thickness in meters of layer	Depth of horizon (mbsl)	Sec TWT of horizon #6900 (GXT1290)	layer thickness in sec TWT	layer Interval velocity (km/s)	sedimentation rate of layer (cm/kyr)
Seafloor	Water (2678)	2678	3.57	3.57	1.5	-
	Dominantly sandstone and claystone at top and bottom (797)			0.84	1.9	15.0
(H7)Top of Miocene		3475	4.4			
	Dominantly claystone with thin sandstone beds (625)			0.6	2.1	4.18
(H6)Top of Oligocene		4100	5.0			
	Claystone with streaks of limestone at bottom (130)			0.1	2.1	1.64
(H5)Top of Eocene		4230	5.1			
	Claystone with streaks of limestone at top and thick sandstone at bottom (330)			0.2	2.4	2.17
(H4) paleocene Unconformity		4560	5.4			
	Dominantly claystone with inter-beds of sandstone at top and bottom (270)			0.2	2.7	3.82
(H3)Top of late cretaceous		4830	5.6			
	Calcareous claystone with sandstone at bottom (670)			0.7	2.6	4.18
(H2) middle cretaceous		5500	6.1			
	Calcareous claystone with siltstone and sandstone (800)			0.5	2.8	5.28
(H1)Top of early cretaceous		6300	6.7			
	Claystone at top and siltstone sandstone and claystone at bottom (751)			0.6	2.9	4.75
Top of crust		7051	7.2			

Table 1: Subsurface lithology and ages at drill site K-1 and the corresponding horizons along the seismic record GXT1290. Interval velocities are from the well logs, while the sedimentation rates are calculated after decompaction of the layers.

Horizon	Lithology and thickness in meters of layer	Depth of horizon (mbsl)	Sec TWT of horizon at #2800 (GXT1290)	layer thickness in sec TWT	Layer Interval velocity (km/s)	Sedimentation rate of layer (cm/kyr)
	water(2962)			3.95	1.5	
Seafloor		2962	3.95			-
	Dominantly claystone and sandstone at top and bottom (1038)			1.0	2.1	19.50
(H7)Top of Miocene		4000	4.95			
	Claystone and inter-bedded sandstone (1370)			0.9	3.0	9.35
(H6)Top of Oligocene		5370	5.85			
	Siltstone at top and claystone with streaks of limestone at bottom (170)			0.1	3.4	-
Top of ridge		5540	5.95			

Table 2: Subsurface lithology and ages at drill site AA and the corresponding horizons along the seismic record GXT1290. Interval velocities are from the well logs, while the sedimentation rates are calculated after decompaction of the layers.

Horizon	Lithology and thickness in meters of layer	Depth of horizon (mbsl)	Sec TWT of horizon (GeoB97-041)	Layer thickness in sec TWT	Layer Interval velocity (km/s)	sedimentation rate of layer (cm/kyr)
Seafloor	water(3133)	3133	4.2	4.2	1.5	-
(H9) Pleistocene unconformity/ Uc	Silty sand and silty clay with numerous turbidites (95)	3228	4.32	0.12	1.58	23.75
	Nannofossil rich clay with silt and foraminifers (60)			0.07	1.71	1.97
(H8) Pliocene Unconformity /Ud		3288	4.39			
	Clayey silt to silty sand Nannofossil rich clay (165)			0.19?	1.74?	10.06
(H7)Top Miocene	of	3453	4.58?			

Table 3: Subsurface lithology and ages at drill site U1444 and the corresponding horizons along the seismic record GeoB97-041. Interval velocities are from the well logs, while the sedimentation rates are calculated after decompaction of the layers.

Integration of recent drill results with multichannel seismic data: New inferences on the subsurface configuration and sedimentary history of the northwestern Bay of Bengal

Supplementary information

Depth to the basement

Depth to the basement at different times is calculated using the equation given by Crosby et al. (2006).

$$\text{depth} = -2821 - (315 * \sqrt{\text{age}})$$

The crustal ages are derived from published literature (Talwani et al., 2016; Desa and Ramana 2016, etc) as shown in Figure 9a. The computed depth is then converted to TWT and plotted in Figures 9b and 9c at 100 Ma and 58 Ma respectively. Sediment load is not considered when analyzing depths for 100 Ma. For 58 Ma, the sediment isopachs are superimposed on the depth to basement map.

The relief of the 85ER is extracted from all the seismic sections from this study as well as published literature. In these records, the average depth surrounding the ridge is considered as 7.5 secs TWT and is subtracted from the basement values to obtain the ridge relief. An amount of 5 sec TWT is considered as subsidence since 108 Ma to obtain the ridge relief at 100 Ma. Figure 9b depicts that the ridge is higher up to 2 secs TWT from the surrounding basement. Thus it is inferred that the ridge was subaerial at 100 Ma.

Synthetic seismogram

The well log data at drill site K-1 was used for obtaining the synthetic seismogram (Figure S3). Sonic data was converted into velocity data, and used along with density data to calculate acoustic impedance. Thereafter, reflection coefficient was calculated. This data was convolved along with a Ricker wavelet of 25 Hz frequency to obtain the synthetic seismogram.

Sedimentation rates

Decompaction of the sediment layers at the drill sites was done by ‘backstripping’ in order to obtain the original thickness of the layers (Sclater and Christie, 1980). Parameters such as original porosity and constant ‘C’ used in the calculation are given in Table S1. Based on the lithology (Tables 1 to 3), these values were varied. Sedimentation rates were then computed at different times using the geological time scale of Gradstein et al. (2012).

Table S1: The parameters used while decompacting the sedimentary layers

Lithology	Original porosity	Constant C/km
sandstone	0.4	0.3
shale	0.5	0.5
limestone	0.45	0.7

Figure captions

Figure S1: Line drawings of published seismic profiles in the study area (a) SK31 (Gopala Rao et al., 1994). Eight horizons (H1 to H8) were identified along this track. (b) MAN-01 (Gopala Rao et al., 1997). In addition to the eight horizons, ages were assigned as follows: B-Upper Pleistocene, A-Miocene, O- Oligocene and P- lower Eocene. (c) SK107-06 (Michael and Krishna, 2011). Ages were assigned to the horizons as follows: H8- lower Eocene, H6- upper Oligocene, H2- upper Miocene, H1- upper Pleistocene (d) GXT1290 (Desa et al., 2013). Horizons Q, M, P were identified as Quaternary base, Miocene top and Paleocene top respectively. In addition layers C, D, E were inferred as Late, Middle and Early Cretaceous respectively. The points of intersection of these profiles with the GXT profiles are indicated as vertical lines. The identifications made in the present study are superimposed onto these profiles. A lot of discrepancy is seen between the identifications in this study and those from published sections. The horizons are coloured as in figures 3 and 5. The locations of the tracks are provided in Figure 2. 85ER: 85°E Ridge; NER: Ninetyeast Ridge

Figure S2: Figure depicting the extent of the Quaternary subfans in the Bay of Bengal (modified from Curray et al., 2003; Bergmann et al., 2019). Subfan A is enclosed in red outline (Curray et al., 2003). For the subfans B to D, the thicker lines (dashed for tentative) indicate the boundaries inferred by Bergmann et al. (2019), while the fine lines in the north are from Curray et al. (2003). Subfan B is

in green (the unhatched portion is tentative), subfan C is in blue and subfan D is in pink. The grey outline is the extent of the entire Bengal Fan. NER: Ninetyeast Ridge; SL: Sri Lanka

Figure S3: The composite figure depicts (a) the subsurface lithology and ages of the major horizons at drill site K-1 modified from Krishna et al. (2016). (b) The seismic record around shot 6900 along the profile GXT1290 at the drill site. (c) The seismic traces at shot 6900. (d) Synthetic seismogram generated using the physical properties obtained from well log information. A fairly good correlation is seen between the seismic traces and seismogram. EC: Early Cretaceous; LC: Late Cretaceous; MC: Middle Cretaceous

References

- Bergmann, F., Schwenk, T., Spiess, V., France-Lanord, C., 2020. Middle to Late Pleistocene Architecture and Stratigraphy of the lower Bengal Fan—Integrating multichannel seismic data and IODP Expedition 354 results. *Geochem. Geophys. Geosys.* 21, e2019GC008702. <https://doi.org/10.1029/2019GC008702>
- Crosby, A.G., McKenzie, D., Sclater, J.G., 2006. The relationship between depth, age and gravity in the oceans. *Geophys. J. Int.*, 166, 553-573.
- Curray, J. R., Emmel, F. J., Moore, D. G., 2003. The Bengal Fan: morphology, geometry, stratigraphy, history and processes. *Mar. Petr. Geol.* 19, 1191-1223.
- Desa, M., Ramana, M. V. Ramprasad, T., Lall, M. V., Kumar, B.J.P., 2013. Geophysical signatures over and around the northern segment of the 85°E Ridge, Mahanadi offshore, Eastern Continental margin of India: Tectonic implications. *J. Asian Earth Sci.* 73, 460-472.
- Desa, M., Ramana, M. V., 2016. Middle Cretaceous geomagnetic field anomalies in the Eastern Indian Ocean and their implication to the tectonic evolution of the Bay of Bengal, *Mar. Geol.* 382, 111–121.
- Gopala Rao, D., Bhattacharya, GC, Ramana, MV, Krishna, K.S., et al., 1994. Analysis of multi-channel seismic reflection and magnetic data along 13°N latitude across the Bay of Bengal. *Mar. Geophys. Res.* 16, 225-236
- Gopala Rao, D., Krishna, K.S., Sar, D., 1997. Crustal evolution and sedimentation history of the Bay of Bengal since the Cretaceous. *J. Geophys. Res.* 102, 17747-17768.
- Gradstein, F. M., Ogg, J. G., Schmitz, M. D., Ogg, G. M., 2012. *The Geologic Time Scale 2012*, 2, Elsevier, Boston, 1176 pp. plus chart.
- Krishna, K.S., Ismaiel, M., Srinivas, K., Gopala Rao, D., Mishra, J., Saha, D., 2016. Sediment pathways and emergence of Himalayan source material in the Bay of Bengal. *Curr. Sci.* 110, 1-12.

Michael, L., Krishna, K.S., 2011. Dating of the 85°E Ridge (northeastern Indian Ocean) using marine magnetic anomalies. *Curr. Sci.* 100, 1314-1322.

Sclater, J.G., Christie, P.A.F., 1980. Continental stretching: An explanation of the post-Mid-Cretaceous subsidence of the Central North Sea Basin. *J. Geophys. Res.*, 85, 3711-3739.

